AERODYNAMIC MODELING AND PERFORMANCE ANALYSIS OF A SHROUDED-FAN UNMANNED AERIAL VEHICLE

Nicola de Divitiis
Department of Mechanics and Aeronautics, University of Rome "La Sapienza"

Keywords: *Unmanned Vehicle, Apparent Mass, Lagrangian*

Abstract

This paper deals with the estimation of the aerodynamic coefficients and performance analysis for a shrouded-fan unmanned aircraft. The complexity of the flow around this kind of vehicles in conjunction with the strong interaction between fan flow and the velocity field about the fuselage, make the aerodynamic coefficients computation a very difficult task. The purpose of this paper is to formulate, by means of the Lagrangian approach, an aerodynamic model for the determination of the aerodynamic coefficients of the shroud, suitable for performance analysis.

1 Introduction

In the last decade the development of Unmanned Aerial Vehicles (UAV) was mainly due to the increasing use of this kind of aircraft in different fields of application.

Several configurations of UAVs have been developed depending upon the required mission profiles [1] and some of them present characteristics quite peculiar with respect to the other ones.

The rotorcraft UAV here considered is a shrouded-fan made of a toroidal hull at the center of which are placed two counter-rotating rotors driven by three two-stroke engines (Fig. 1). The vehicle performance characteristics are reported in Tab.1.

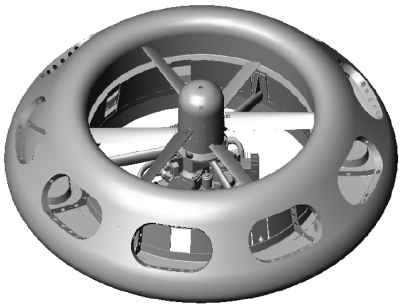

Fig. 1 UAV configuration

Overall diameter (m)	1.9
Rotor diameter (m)	1.1
Central hub diameter (m)	0.25
Maximum Overall weight (N)	800
Payload (N)	100
Coaxial rotors	2
Power ($h.p.$)	3×14
at (RPM)	11000
Rotor speed (RPM)	3000
Endurance (h)	1.5
Service ceiling (m)	2000

Table 1. Characteristics of the UAV.

In a previous work [2], focused on performance and stability of a shrouded UAV, in order to build the aerodynamic model, the aerodynamic actions developed by the shroud, were estimated by means of computational fluid dynamics using the code VSAERO for various flight conditions and it was remarked that, because of the the strong interaction between rotor flow and aerodynamic field on the hull, the evaluation of the

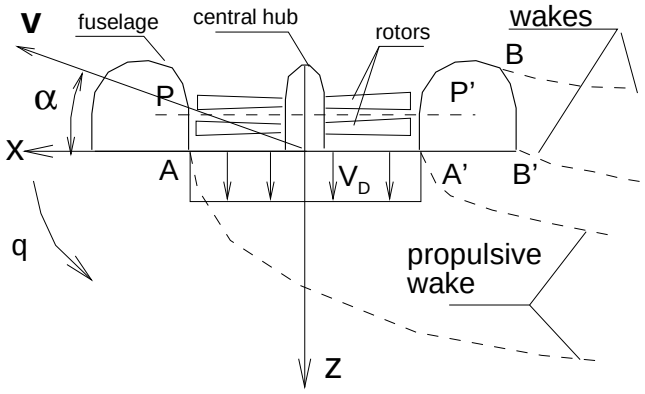

Fig. 2 UAV aerodynamics in forward flight

aerodynamic coefficients for any flight condition is a difficult task.

Taking into account the great excursion of the angle of attack ($-90 < \alpha < +90$ *deg*), depending on flight conditions, quite different aerodynamic field structures around the UAV can develop [3] and consequently the performance analysis of the vehicle requires an accurate modelization of the flow field on a wide range of variation of the angle of attack. The rotorcraft configuration here treated, very similar to that considered in Ref. [2], is the result of a parametric study, realized by means of the code VSAERO, which analyzes the forces developed by different geometries of toroidal fuselage in the presence of the rotor flow. The chosen fuselage cross section corresponds to

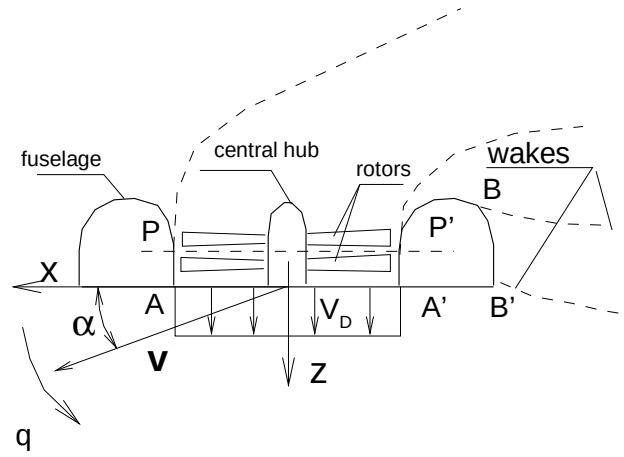

Fig. 3 UAV aerodynamics: Windmill brake state

achieve low values of the pitch moment in a wide range of angle of attack together to drag coefficients less than those calculated in [2].

An aerodynamic model for the determination of the aerodynamic coefficients of the UAV configuration in the presence of the interaction between hull and rotors is developed. This model, based upon the apparent mass concept, requires the definition of a Lagrangian function representing the kinetic energy of the flow expressed in terms of the UAV state variables and allows the calculation of aerodynamic forces and moments through the method of the Lagrange equations.

The effects of the rotor flow on the aerodynamic field about the airframe are accounted for by modeling the rotors using an actuator disk with a properly calculated doublet distribution.

Due to its physical derivation, the aerodynamic model takes into account the aforementioned effects which regard the mutual interaction between the rotor flow and the aerodynamic field about the rotorcraft.

As a successive step, in order to calculate both thrust and rotor torque, a rotor model is adopted which takes into account the variations of collective and cyclic pitch for various flight conditions. This model determines, by using steady-state aerodynamics analysis, the thrust and the moment coefficients by integration of the aerodynamic load along the blade span.

Finally, the results of a detailed study of performance characteristics for straight and turning flight conditions, such as control angles, required power and flight path angles as a function of speed are discussed.

2 Vehicle Modeling

In order to develop the aerodynamic model, one has to model the flow field about the UAV.

First of all, due to the axial symmetry around the z axis, the flow about the hull depends on α and on the rotors induced velocity V_D. Therefore it can be shown that the aerodynamic coefficients are functions of α, p,q,r and of the ratio $k = \dfrac{V}{|V_D - V\sin\alpha|}$ and do not depend on the sideslip angle.

Figures 2 and 3 show two possible schemes of the flow structures that are possible during the flight.

Figure 2 shows the UAV section in the condition of *normal working state* which corresponds to flight situations in which the angle of attack is negative and V_D is sufficiently greater than $V\sin\alpha$. In this working regime the rotor inflow from the top of the aircraft, the fluid is ejected towards the bottom and the power is transfered from the rotors to the air. The rotor flow and the external stream are separated by a potential wake which originates from the separation line that is represented by A and A'.

Another possible schematic of the UAV aerodynamics is represented in Fig. 3, where the angle of attack is positive and the induced velocity V_D is low enough with respect to $V\sin\alpha$ to permit an upward flow relative to the rotor that causes the so called *windmill-brake state* where the power is transfered from the stream to the rotor.

These two conditions, in accordance to the Ref. [2], also consider the presence of wakes attached behind the fuselage on the separation lines B and B'.

More complicate flow structures such as the *turbulent wake state* or the *Vortex ring state* [3], which correspond to different flight conditions, could be verified in intermediate situations that are not accounted for in the present study.

In both cases, angle of attack and angular velocity influence all the aerodynamic coefficients, whereas the presence of the rotor flow significantly contributes to modify the aerodynamic field about the fuselage so as to made the vehicle aerodynamics quite different from that of a conventional rotorcraft. In order to take into consideration the influence of the rotor flow about the airframe, in the adopted scheme, the rotors are subsituted by suitable equivalent actuator disk placed the mid plane PP' (Figs. 2, 3). Therefore, the rotor flow is supposed to be generated by a layer of doublets placed in PP' with a properly calculated induced velocity V_D. The velocity V_D is an unknown parameter that depends upon the rotor working conditions and is determined by means of the rotor model, described in the following, together with the impulsive theory.

It is worth to remark that the influence of V_D on the entire aircraft represents the effects of the collective pitch on the aerodynamic field about the vehicle while the cyclic pitch variation, which in turn causes a non-uniform distribution of V_D is not accounted for.

As far as the propulsive system, the thrust force is obtained by the two rigid (no flapping) counter-rotating rotors which in turn have the purpose to control the vehicle attitude. In particular pitch and roll are controlled through longitudinal δ_B and lateral δ_A variations of blade pitch, whereas yaw control is carried out by means of differential variations δ_P of the collective pitch on the two rotors whose angular velocity is kept constant by a RPM governor. The blade pitch is controlled by a mechanism consisting in two independent swash-plates, each controlled by three actuator.

The rigidity of the two rotors causes moments that are transmitted from the rotors to the airframe and that they will must be compensated by a proper action on the controls.

Thrust force and moment are obtained through a model, that assumes a constant rotor speed, based on the application of the blade element theory for each blade.

The rotor model here used, that is the same one employed in [2], calculates the thrust forces and moments through an analytical integration of the rotor load along the blade span by assuming steady state aerodynamics for the rotors, while the effects due to the blade-tip losses and the mutual influence between the two rotors are neglected.

3 Aerodynamic Model

A method to calculate the aerodynamic forces on the fuselage of the UAV configuration, is now presented. This procedure has been already successfully applied to the calculation of the aerodynamic forces of ultralight vehicles [4] and of ultralight sailplanes in the presence of a wind gradient [5].

In order to derive the accurate expressions of the aerodynamic forces and moments, it is con-

sidered that the UAV is in a potential flow. The expression of the kinetic energy of the stream is [6]

$$T = \frac{1}{2}\rho \int\int_{S_w} \phi\, \mathbf{n}\cdot\mathbf{v}\, dS + \frac{1}{2} V\, t\rho \int_{\Gamma_1} \phi\, \mathbf{n}\cdot\mathbf{v}\, dl + \frac{1}{2}\frac{|\mathbf{v}+\mathbf{v}_2|}{2}\, t\rho \oint_{\Gamma_2} \phi\, \mathbf{n}\cdot\mathbf{v}\, dl \tag{1}$$

where ϕ is the potential flow, S_w is the fuselage wetted surface, $\mathbf{n}$ is the unit vector normal to the local surface, whereas $\mathbf{v}$ and $\mathbf{v}_2$ are, respectively, the aircraft velocity expressed in body axes and the induced velocity by rotor flow at the downstream infinity. In the calculation of $\mathbf{v}_2$ the possible swirl effects caused by the rotors are not accounted for. In accordance to the potential flow theory, the first term of Eq. (1) is the kinetic energy of the air moved by the aircraft, whereas the second and the third ones, that under the steady-state hypothesis result linear functions of time, are integrals path along the separation lines Γ_1 and Γ_2 respectively and represent the contribution of possible wakes to the kinetic energy. In particular Γ_1, indicated as BB' in the Fig. (2) and (3), is the line where the wake originates on the rotorcraft hull while Γ_2, indicated as AA', corresponds to the circumference of both the rotor disks.

Now, since the potential ϕ is solution of the Laplace equation (linear), it can be expressed through the sum of different terms due to flight velocity $\mathbf{v}$, angular velocity ω and induced velocity of the rotor system V_D *i.e.*

$$\phi = \frac{\partial\phi}{\partial\mathbf{v}}\cdot\mathbf{v} + \frac{\partial\phi}{\partial\omega}\cdot\omega + \frac{\partial\phi}{\partial V_D}\, V_D \tag{2}$$

where the terms $\frac{\partial\phi}{\partial\mathbf{v}} \equiv (\frac{\partial\phi}{\partial u}, \frac{\partial\phi}{\partial v}, \frac{\partial\phi}{\partial w})$ and $\frac{\partial\phi}{\partial\omega} \equiv (\frac{\partial\phi}{\partial p}, \frac{\partial\phi}{\partial q}, \frac{\partial\phi}{\partial r})$ discussed in detail in Lamb [6], are the potential per unit flight velocity and per unit angular velocity respectively, while the last term is the potential per unit V_D which gives the contribution of the doublet distribution on the plane PP'.

Substituting Eq. (2) into Eq. (1) one obtains the kinetic energy expression of the stream in terms of $\mathbf{v}$, ω and V_D

$$T = [\tfrac{1}{2}\mathbf{v}\cdot\mathbf{M}\mathbf{v} + \tfrac{1}{2}\omega\cdot\mathbf{J}\omega + \tfrac{1}{2}V_D\,\mathbf{g}\cdot\mathbf{v} + (\tfrac{1}{2}\mathbf{v}\cdot\dot{\mathbf{M}}\mathbf{v} + \tfrac{1}{2}\omega\cdot\dot{\mathbf{J}}\omega + \tfrac{1}{2}V_D\,\dot{\mathbf{g}}\cdot\mathbf{v})\, t]\rho \tag{3}$$

The first addend of Eq. (3) contains $\mathbf{M}$ and $\mathbf{J}$ which are two symmetric and defined positive tensors that, when expressed in body axes, do not depend on the angle of attack while $\mathbf{g}$ represents the term related to the effects of the rotor flow. $\rho\mathbf{M}$ and $\rho\mathbf{J}$, since their dimensions and physical meaning, are called apparent mass terms. The second term of Eq. (3), that is a linear function of time, derives from the second and the third addends of Eq. (1) and contains the quantities $\dot{\mathbf{M}}$, $\dot{\mathbf{J}}$ and $\dot{\mathbf{g}}$ that formally are the time derivative of $\mathbf{M}$ and $\mathbf{J}$ and $\mathbf{g}$ respectively. Now, according to Eq. (1), $\dot{\mathbf{M}}$, $\dot{\mathbf{J}}$ and $\dot{\mathbf{g}}$ have the same form that depend upon V and V_D

$$\begin{aligned} \dot{\mathbf{M}} &= [V\,\mathbf{M}_1 + \frac{|\mathbf{v}+\mathbf{v}_2|}{2}\mathbf{M}_2]\rho \\ \dot{\mathbf{J}} &= [V\,\mathbf{J}_1 + \frac{|\mathbf{v}+\mathbf{v}_2|}{2}\mathbf{J}_2]\rho \\ \dot{\mathbf{g}} &= [V\,\mathbf{g}_1 + \frac{|\mathbf{v}+\mathbf{v}_2|}{2}\mathbf{g}_2]\rho \end{aligned} \tag{4}$$

where $\mathbf{M}_1$, $\mathbf{J}_1$, $\mathbf{g}_1$ and $\mathbf{M}_2$, $\mathbf{J}_2$, $\mathbf{g}_2$ are two groups of arrays that give the influence of the wakes which start form BB' and AA' respectively.

The induced velocity by rotor flow at the downstream infinity $\mathbf{v}_2$ has been calculated in terms of V_D through the impulsive theory [3]

$$\frac{\mathbf{v}_2{}^2 - \mathbf{v}^2}{2} = V_D(\sqrt{\mathbf{v}_2{}^2 - \mathbf{v}^2\cos^2\alpha} - |\mathbf{v}|\sin\alpha) \tag{5}$$

and, when axial flight occurs, Eq. (5) provides the well known result $V_D = \frac{|\mathbf{v}| + |\mathbf{v}_2|}{2}$.

The aerodynamic force $\mathbf{F}$ and moment $\mathbf{Q}$ on the fuselage are obtained using the Lagrange

equations in the general form [6]

$$\begin{aligned}\mathbf{F} &= -\frac{d}{dt}\frac{\partial T}{\partial \mathbf{v}} - \omega \times \frac{\partial T}{\partial \mathbf{v}} \\ \mathbf{Q} &= -\mathbf{v} \times \frac{\partial T}{\partial \mathbf{v}} - \frac{d}{dt}\frac{\partial T}{\partial \dot{\omega}} + \frac{\partial T}{\partial \omega}\end{aligned} \tag{6}$$

Substituting Eq. (1) into Eq. (6), one obtains

$$\begin{aligned}\mathbf{F} &= -[\mathbf{M}\dot{\mathbf{v}} + \omega \times \mathbf{M}\mathbf{v} + \frac{V_D}{2}\omega \times \mathbf{g} + \dot{\mathbf{M}}\mathbf{v} \\ &\quad + \frac{V_D}{2}\dot{\mathbf{g}}]\rho \\ \mathbf{Q} &= -[\mathbf{J}\dot{\omega} + \omega \times \mathbf{J}\omega + \mathbf{v} \times \mathbf{M}\mathbf{v} + \dot{\mathbf{J}}\omega \\ &\quad + \frac{V_D}{2}\mathbf{v} \times \mathbf{g}]\rho\end{aligned} \tag{7}$$

It is interesting to analyze the terms which appear in the first of Eqs. (7). $\mathbf{M}\dot{\mathbf{v}}$, usually neglected in flight dynamics, represents the inertia force of the air flow that, in the present application, results $\rho|\mathbf{M}\dot{\mathbf{v}}|/|m\dot{\mathbf{v}}| << 1$. This is because $\mathbf{M}$, which represents the air mass moved by the rotorcraft fuselage, results much less than rotorcraft mass and for this reason it will be neglected in the present study. $\omega \times \mathbf{M}\mathbf{v}$, which depends on both flight velocity and angular velocity, is the contribution of the rotary derivative to the aerodynamic force whereas $\frac{V_D}{2}\omega \times \mathbf{g}$ gives the simultaneous effects of angular velocity and rotor flow (collective pitch). $\dot{\mathbf{M}}\mathbf{v}$, which depends upon the angle of attack and flight velocity, is the steady-state term of the aerodynamic force. Finally $\frac{V_D}{2}\dot{\mathbf{g}}$, gives the influence of the rotor flow on the aerodynamic force.

As for the second of Eqs. (7), $\mathbf{J}\dot{\omega}$ is a moment term due to the inertia force of the air flow that, due to its smaller order of magnitide with respect to the rotorcraft moments of inertia, will be not considered in the moment balance. Both $\omega \times \mathbf{J}\omega$ and $\dot{\mathbf{J}}\omega$ represent the contribution of the moment rotary derivatives, while $\mathbf{v} \times \mathbf{M}\mathbf{v}$, that depends upon flight speed and angle of attack, is the steady-state aerodynamic moment. $\frac{V_D}{2}\mathbf{v} \times \mathbf{g}$ gives the contribution of the rotor flow on the aerodynamic moment.

Eqs. (7) state that $\mathbf{M}$, $\mathbf{J}$, $\dot{\mathbf{M}}$, $\dot{\mathbf{J}}$ are the aerodynamic derivatives of force $\mathbf{F} \equiv (X,Y,Z)$ and moment $\mathbf{Q} \equiv (L,M,N)$ with respect to the acceleration and velocity components, respectively. Therefore they can be expressed in terms of aerodynamic derivatives. For instance the matrix $\dot{\mathbf{M}}$ can be written as

$$\dot{\mathbf{M}} = \begin{bmatrix} -\frac{\partial X}{\partial u} & -\frac{\partial X}{\partial v} & -\frac{\partial X}{\partial w} \\ -\frac{\partial Y}{\partial u} & -\frac{\partial Y}{\partial v} & -\frac{\partial Y}{\partial w} \\ -\frac{\partial Z}{\partial u} & -\frac{\partial Z}{\partial v} & -\frac{\partial Z}{\partial w} \end{bmatrix} \tag{8}$$

Due to the axial symmetry of the fuselage, the aerodynamic force and moment expressed in body axes, are written in the form

$$\begin{aligned}\mathbf{F} &= \frac{1}{2}\rho V_f^2 S\, \mathbf{L}_{BW}(\alpha,\beta_x)(-C_D,\ 0,\ -C_L) \\ \mathbf{Q} &= \frac{1}{2}\rho V_f^2 S d_f\, \mathbf{L}_{BW}(\alpha,\beta_x)(0,\ -C_m,\ 0)\end{aligned} \tag{9}$$

where d_f is the shroud diameter, $S = \pi d_f^2/4$ is the reference surface, $V_f = \sqrt{u^2+v^2+(w-V_D)^2}$ is the reference velocity in which u, v and w are the flight velocity components in body axes while $\mathbf{L}_{BW}(\alpha,\beta_x)$ is the transformation matrix from wind to body axes. Here, the aerodynamic angles α and β_x are defined as

$$\begin{bmatrix} u \\ v \\ w \end{bmatrix} = V \begin{bmatrix} \cos\alpha\ \cos\beta_x \\ \cos\alpha\ \sin\beta_x \\ \sin\alpha \end{bmatrix} \tag{10}$$

Both Eqs. (7) and (9) provide the aerodynamic coefficients in terms of α and k. Unfortunately, due to Eq. (5) the aerodynamic coefficients can not be expressed in closed form as functions of α and k. Nevertheless it is possible to evaluate the aerodynamic force and moment coefficients by solving numerically Eqs. (7) and (9) in the entire range of variation of α and k.

It is worth to remark that, in hovering Eqs. (7) and (9) yield

$$\begin{aligned} C_x = C_y = 0,\ C_z = \frac{2\, g_{2\,z}}{S} \\ C_l = C_m = C_n = 0 \end{aligned} \tag{11}$$

Eq. (11) states that, when the flight speed is equal to zero the aerodynamic coefficients do not depend upon the angle of attack which, in this situation, is undetermined. This is in accordance with the fact that, in the hovering condition, forces and moments coefficients developed by the shroud have unique values. This is a fundamental property that must be taken into account from any aerodynamic model.

The advantage of the present model with respect to a database in tabular form is related to its physical derivation which permits to take into consideration the physical aspects that characterize the aerodynamic forces acting on the airframe.

Furthermore, since Eqs. (3) are mathematically defined on the entire domain of variations of α and k, the model allows to determine the aerodynamic force and moment coefficients in any flight condition.

4 Modeling Identification

This section deals with the identification of the model parameters.

As seen, the quantities $\mathbf{M}$, $\mathbf{M}_1$, $\mathbf{M}_2$, $\mathbf{J}$, $\mathbf{J}_1$, $\mathbf{J}_2$, $\mathbf{g}$, $\mathbf{g}_1$, $\mathbf{g}_2$ depend on the vehicle geometry and can be determined through integration on the airframe surface of the velocity potential ϕ or they can be identified through computational fluid dynamics or by means of wind tunnel tests.

The elements of these matrices are the free parameters of the proposed model. They have been identified through the elaboration of data obtained by means of CFD simulations using the code VSAERO by Analytical Methods, Inc.[7] which permits to take into account different flight conditions. In particular, the influence of the potential wakes is taken into account through a wake-relaxation scheme while the influence of the rotors flow on the hull is calculated by means of a simple propeller-slipstream routine. The boundary layer effects are determined by subroutines that calculate the boundary layer quantities on the overall wetted surface.

Consequentely, the separation lines on the fuselage are located where the skin friction is vanishing.

Therefore, to identify the free parameters, several CFD simulations have been carried out.

The identification of the free parameters is achieved by means of an optimization procedure based on the least-square method that satisfies the condition

$$J = \frac{1}{2}\sum_k [(C_k)_{CFD} - C_k]^2 \;=\; min \tag{12}$$

where $(C_k)_{CFD}$ is the value of the generic aerodynamic coefficient obtained by the CFD simulations whereas C_k is the aerodynamic coefficient calculated through Eq. (7).

5 Equations of Motion

This section deals with the equations of motion for the rotorcraft which are written as [8]

$$\begin{aligned} &m(\dot{\mathbf{v}} + \boldsymbol{\omega} \times \mathbf{v}) = \mathbf{F} + \mathbf{F}_T + m\mathbf{L}\mathbf{g}, \\ &\mathbf{I}\dot{\boldsymbol{\omega}} + \boldsymbol{\omega} \times \mathbf{I}\boldsymbol{\omega} = \mathbf{Q} + \mathbf{Q}_T \\ &\dot{\mathbf{r}} = \mathbf{L}^T\mathbf{v}, \quad \dot{\Phi} = \mathbf{R}^{-1}\boldsymbol{\omega} \end{aligned} \tag{13}$$

where $m\mathbf{Lg}$ is the weight force expressed in body axes while $\mathbf{F}_T$ and $\mathbf{Q}_T$ are the thrust force and moment generated by the rotors expressed as

$$\begin{aligned} &\mathbf{F}_T = -\pi\,\rho\,\Omega^2\,R^4\,(C_{x_T}, C_{y_T}, C_{z_T}) \\ &\mathbf{Q}_T = \pi\,\rho\,\Omega^2\,R^5\,(C_{l_T}, C_{m_T}, C_{n_T}) \end{aligned} \tag{14}$$

where the nondimensional coefficients in Eqs. (14) are determined through the rotor model used in Ref. [2]. Since the two rotors have the same moments of inertia with respect to the rotation axis and are counter-rotating, the corresponding moments induced by the gyroscopic effects on the airframe are balanced and, therefore, do not appear in the rigid body moment equations.
The last two of Eqs. (13) are the navigation equation and the attitude equation, where $\mathbf{r}$ represents the $c.g.$ location whereas $\Phi = (\varphi, \vartheta, \psi)$ and $\mathbf{R}^{-1}$ are, respectively, the Euler angles vector and the transformation matrix from $\boldsymbol{\omega}$ to $\dot{\Phi}$.

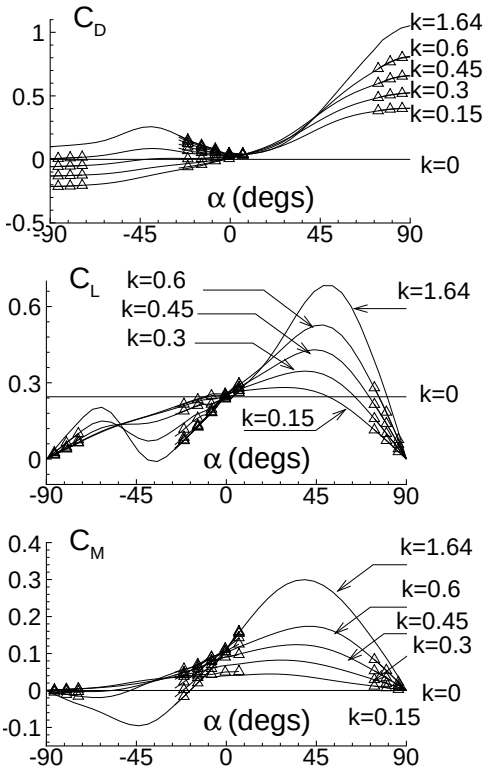

Fig. 4 Aerodynamic coefficients

6 Results and Discussion

First, the results which concern the identification of the free parameters of the aerodynamic model are presented.

In order to identify the free parameters, several CFD calculation at $p = q = r = 0$ has been carried out in the three range of variation of $\alpha \times k$ $A_1 = [-26,\ 25] \times [0.2,\ 1.64]$, $A_2 = [74,\ 90] \times [0.15,\ 0.6]$ and $A_3 = [-90,\ -74] \times [0.15,\ 0.6]$ that correspond, respectively, to forward flight at small angle of attack, descending and climbing flight. Moreover, in order to take into account the effects of the angular velocities, three series of CFD calculation, each obtained for $\omega = (p,0,0),(0,q,0),(0,0,r)$, have been realized. Figure 4 shows the aerodynamic coefficients *vs* α at different values of k. The continuous lines correspond to the aerodynamic coefficients C_k, obtained by the present model, whereas the symbols represent $(C_k)_{CFD}$. All the free parameters are calculated via Eq. (12), so that the aerodynamic coefficients are defined and can be calculated through the proposed model. In any situation the difference between $(C_k)_{CFD}$ and C_k is less than 3% and this coresponds to obtain a minimum value of J less than 10^{-5}. This little value means that Eqs. (7) fit very well the CFD calculations and therefore, at least from potential

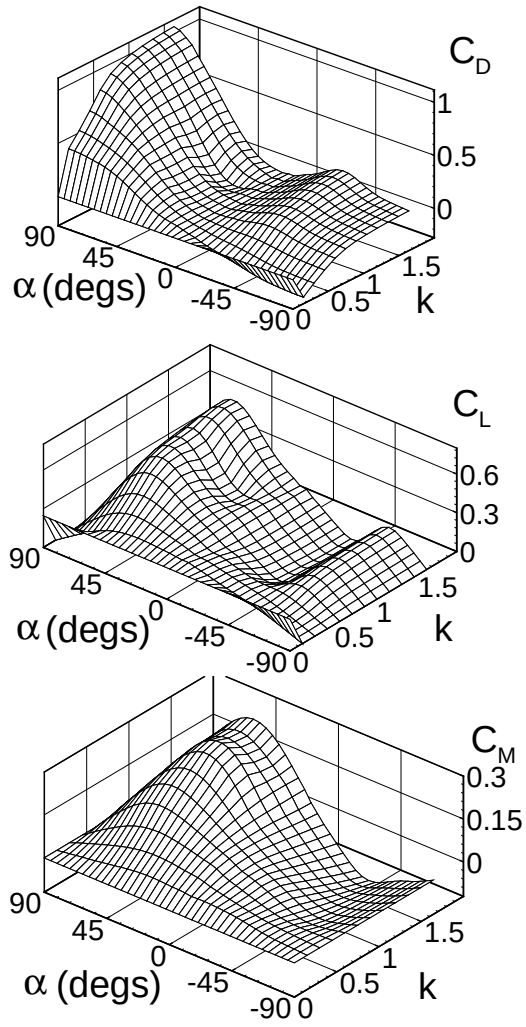

Fig. 5 Aerodynamic coefficients vs. α and k

flow standpoint, it describes in adequate fashion the UAV aerodynamics. The result of the model identification are shown in Fig. 5 where the three surfaces represent lift, drag and pitch moment coefficients in the entire range of variation of α and k. As previously observed, for $k = 0$ (hovering condition), each aerodynamic coefficient does not depend on the angle of attack.

Now, the results of the trim analysis in the straight and turning flight at different flight speeds will be presented. The trim conditions are calculated by solving the steady-state motion

equations through a minimization procedure with assigned constraints [9]. From previous results given in [2] and the UAV Cypher data [1], it is apparent that the maximum speed of this kind of

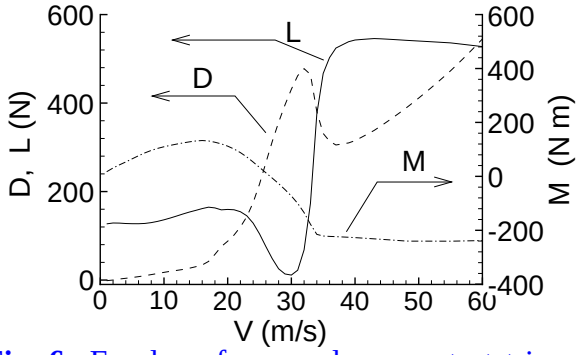

Fig. 6 Fuselage force and moment at trim vs. flight speed

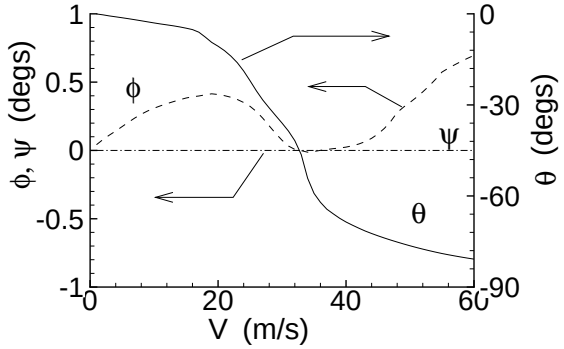

Fig. 7 Euler angles vs. flight speed

vehicle does not exceed 30 $m\ s^{-1}$. Nevertheless, in order to investigate the rotorcraft performance in a wider envelope, the flight speed will be considered variable in the range $0 < V < 60\ m\ s^{-1}$ while the sideslip angle is put equal to zero.

The plots in Fig. 6 represent drag, lift and pitch moment developed by the hull, calculated in the trim conditions. Both pitch moment and drag force, due to the different fuselage shape, result less than those given in Ref. [2]. The pitch moment exhibits a maximum value at 15 $m\ s^{-1}$ which corresponds to an angle of attack of about 6 *deg*. At higher velocity, the moment increases up to a speed of 35 $m\ s^{-1}$ where, due the simultaneous variations of flight speed and the angle of attack, it assumes an almost constant value.

The pitch moment will be balanced by the moments developed by control actions. For what concerns the lift developed by the shroud, the adopted fuselage seems to be able to develop a high level of lift which contributes to balance

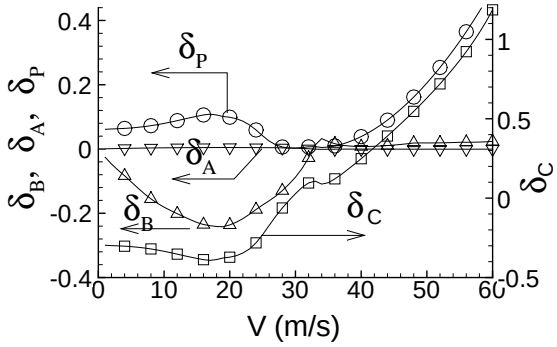

Fig. 8 Controls angles vs. flight speed

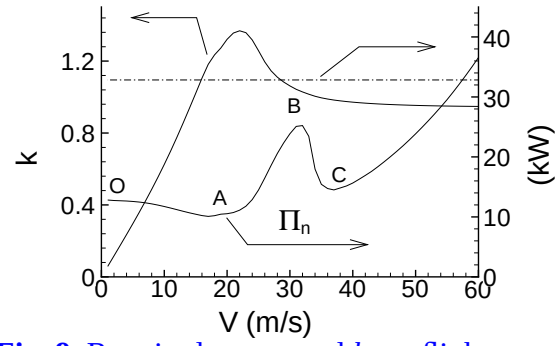

Fig. 9 Required power and *k* vs. flight speed

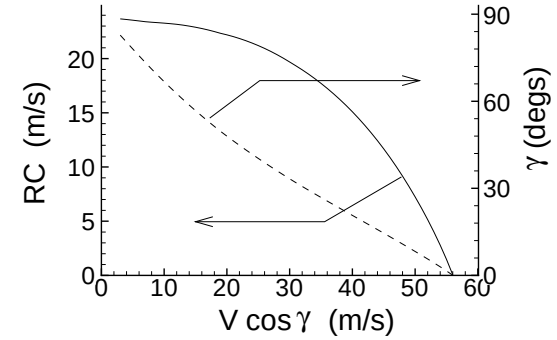

Fig. 10 Rate of climb and flight path angle vs. flight speed

part of rotorcraft weight in a wide range of flight velocity. In particular, at slow speed, when the angle of attack is small, the lift contribution is not significant with respect to the thrust force whereas, for velocities greater than 30 $m\ s^{-1}$, the lift achieves the value of 580 N which represents more than 70% of the vehicle weight. This optimistic result, which seems to
predict a high vehicle performance, is directly related to the fuselage aerodynamics and should be verified through wind tunnel tests. Also the drag presents some peculiarities. For velocities until

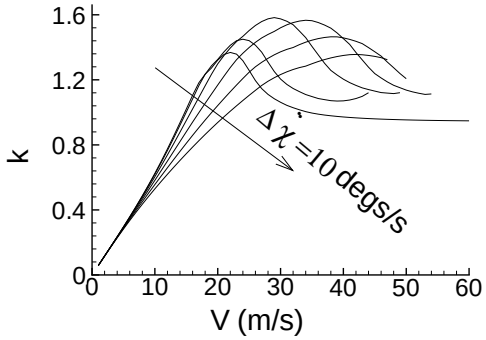

Fig. 11 *k* vs. flight speed at different turn rate

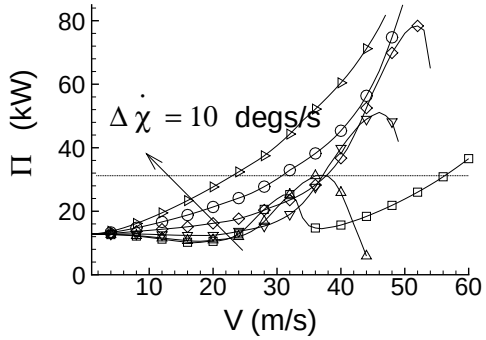

Fig. 12 Required power vs. flight speed at different turn rate

to 20 $m\ s^{-1}$ the drag remains limited while for $20 < V < 30\ m\ s^{-1}$ it quickly rises to reach its maximum value at $V = 30\ m\ s^{-1}$. In the interval $30 < V < 37\ m\ s^{-1}$ it has a significant reduction and then, for higher velocities, shows a monotonic behavior. These lift and drag variations are explained through the non-linearity of the aerodynamic model.

Figure 7 shows the Euler angles as the functions of the forward speed. In particular, in accordance to [2], the roll angle φ, due to the differential pitch which acts through the collective on both the rotors, is different from zero. Nevertheless, because of the rotors are counter-rotating, φ, is very small in the entire range of speed variation. The pitch angle ϑ varies from 0 until to about 80 *deg* thanks to the aforementioned lift hull capabilities.

As far as the controls are concerned, Fig. 8 shows, in the trim conditions, δ_B, δ_A, δ_P, δ_C *vs.* the flight speed. The collective pitch δ_C, that controls the thrust force, presents sizeable variations. It is relatively small for speed less than 35 $m\ s^{-1}$ whereas, for higher velocities, it increases up to values that could be not feasible from the control system. Therefore the vehicle performance, in particular maximum flight speed and rate of climb, depend upon both maximum delivered power and maximum collective pitch. The longitudinal cyclic δ_B balances the pitch moment developed by the shroud, whereas the differential collective δ_P, varies in such a way to compensate the torque produced by the engines. Because of the symmetric flight conditions, the lateral cyclic δ_A is always equal to zero.

In Fig. 9, the required power Π_n and k are presented. This plot directly depends on the aerodynamic forces developed at trim. Π_n is greater than zero for $V = 0$ and, due to the non-linear aerodynamics, it presents two decreasing tracts, *OA* for velocities less than 20 $m\ s^{-1}$ and *BC* in the interval $30 < V < 35 m\ s^{-1}$, which correspond to flight conditions with propulsive instabilities. The tract *OA*, very similar to the helicopter power law, is lightly different from that calculated in [2] due to the different fuselage. As for k, for velocities that do not exceed the 30 $m\ s^{-1}$, the diagram is very similar to that one given by Ref. [2] whereas, for higher forward speed, k lightly decreases.

At this point we can state that the non-linearity of the rotrocraft model seems to cause two flight regimes, one of which, for $V < 30\ m\ s^{-1}$, is similar to that one obtained in Ref. [2]. The other one, obtained for $V > 30\ m\ s^{-1}$, seems to be related to the lift developed by the hull (see Fig. 6) which significantly contributes to balance the rotorcraft weight.

In order to study the UAV climb performance, the rate of climb *RC* and the flight path angle γ as the functions of the forward velocity, are analyzed. Fig. 10 reports the hodograph of climbing flight and the flight path angle. Also in this situation each flight condition is evaluated by the same minimization method explained in [9]. Due to the relatively high excess power-weight ratio ($0.027\ kWN^{-1}$) with respect to high performance helicopters ($0.013\ kWN^{-1}$ for the KA 32), the *RC* so calculated, is about two times greater than the maximum RC for high performance helicopters. Of course this result is the consequence of the

performance analysis, hence it has to be verified against on the feasibility of some parameters such as the blades angles of attack and the controls. In all the flight conditions reported in Fig. 10, the blades angle of attack is less than 11 *deg* whereas control displacements never exceed their maximum values.

A further analysis concerns the UAV performance in turning flight. Figures 11 and 12 show k and Π_n *vs.* V where each curve is calculated for an assigned turn rate $\dot{\chi}$ which starts from $\dot{\chi} = 0$ until to $\dot{\chi} = 50\ deg\ s^{-1}$ with an increase $\Delta\dot{\chi} = 10\ deg\ s^{-1}$, while the sideslip angle is kept equal to zero. As the turn rate increases, Π_n and k vary in such a way that both power excess and maximum speed reduce their values. For $\dot{\chi} > 20\ deg\ s^{-1}$, because of the inertia forces, Π_n significantly increases and exhibits a monotonic variation law. The blades angle of attack is always less than 11 *deg* and control displacements do not exceed their maximum values.

7 Conclusion

We conclude by summarizing some of the significant results of the present work.

To analyze the UAV performance, a method that allows to calculate the aerodynamic coefficients developed by the fuselage of rotorcraft, is proposed. The model is based upon the potential representation of the flow field about the UAV. The aerodynamic model requires the definition of the Lagrangian function, expressed in terms of some matrices, the elements of which are the model free parameters calculated through an identification procedure based on the elaboration of data obtained by CFD simulations. In spite of the presence of complicate flow structures about the vehicle, this approach is supposed to hold in all the flight situations. This is the main limitation of the model because the calculation of the aerodynamic coefficients and the consequent performance analysis are valid under the assumption that the flow structures about the vehicle are represented by *normal working state* and *windmill-brake state*. More complicate flow structures such as *turbulent wake state* or the *Vortex ring state* can not be taken into account from a Lagrangian approach which derives from a potential field formulation. Therefore, in the performance analysis the assumption which regards the *normal working state* and *windmill-brake state* must be verified *a posteriori*.

8 Acknowledgment

The author would like to thank Professor Guido de Matteis for his helpful suggestions.

References

[1] Walsh, D. and Cycon J.P., "The Sikorsky Cypher UAV: A Multi-purpose Platform with Demonstrated Mission Flexibility", Proceedings of the annual Helicopter Society pp. 1410-1418.

[2] Avanzini G., D'Angelo S., de Matteis G. "Performance and Stability of a Ducted-Fan Uninhabited Aerial Vehicle. AIAA-2001-0844.

[3] Newman S. *The Foundation of Helicopter Flight*, Ed. Arnold editor, 1994, pp. 49-62.

[4] de Divitiis N., "Performance and Flying Qualities of Ultralight Aircraft", XV AIMETA Congress of Theoretical and Applied Mechanics

[5] de Divitiis N. "Effect of Microlift Force on the Performance of Ultralight Aircraft", *Journal of Aircraft* Vol.39, no.2 pp.318-325.

[6] Lamb, H., "On the Motion of Solids Through a Liquid", *Hydrodynamics*, 6th ed., Dover, New York, 1945, pp. 160-201.

[7] Analytical Methods Inc. VSAERO User's Manual. Revision E5, April, 1994, pp. 1-52.

[8] Etkin, B., *Dynamics of Atmospheric Flight.* John Wiley & Sons, New York, 1972, pp. 104, 152.

[9] Stevens, B.L., and Lewis, F.L. *Aircraft Control and Simulation*, John Wiley & Sons, New York, 1992.